Comparative studies of Coulomb barrier heights for nuclear models applied to sub-barrier fusion

W. W. Qu,[1,2] G. L. Zhang,[1,2,*] H. Q. Zhang,[3] and R. Wolski[4]

[1]*School of Physics and Nuclear Energy Engineering, Beihang University, Beijing 100191, China*

[2]*International Research Center for Nuclei and Particles in the Cosmos, Beihang University, Beijing 100191, China*

[3]*China Institute of Atomic Energy, Beijing 102413, China*

[4]*Henryk Niewodniczański Institute of Nuclear Physics PAS, Cracow 31-342, Poland*

(Received 9 September 2014; revised manuscript received 21 October 2014; published 2 December 2014; corrected 29 December 2014)

Coulomb barrier heights provided by different nuclear interaction models including the Bass model, the proximity potential model, and the double folding model have been applied for experimental data of fusion in terms of a recently proposed energy scaling approach. The results show that the proximity potential description of the barrier heights seems to be closest to the values required by the systematics. It is suggested that the proximity potential model is the most suitable model to calculate the barrier height. However, the double folding model gives the lowest barrier heights.

DOI: 10.1103/PhysRevC.90.064603 PACS number(s): 25.70.Jj, 25.70.Gh, 24.10.−i

I. INTRODUCTION

Heavy ion fusion is an important issue in nuclear physics [1–4]. With the development of the radioactive ion beam (RIB) which can produce neutron-rich and proton-rich nuclei, particular interest has been paid to the production and decay of superheavy nuclei. As a result, fusion reactions using RIB have reattracted much attention to date and the new phenomena were observed, which gives challenges for theoretical models [5–7].

For many fusion reactions in the experiments mentioned in the literature, the barrier height is the basic parameter for describing the fusion. One usually measures some observable quantities to provide barrier parameters in terms of specific interpretation. The different models such as the Bass model, proximity potential, and double folding model are used to calculate the nuclear potentials for fusion reactions to obtain the Coulomb barrier heights [8–12]. Moreover, on the basis of the calculated results, the parametrized formula of Coulomb barrier heights can be obtained [13–15]. However, it is hard to say which model is suitable for fusion reaction.

There have been many experiments on fusion reactions. Some examples show that, at sub-barrier energies, the deformation effect of nuclei related to collective excitation of colliding nuclei would affect the fusion process [16]. However, many experiments show the enhancement at sub-barrier energies due to positive Q-value neutron transfer (PQNT) [17]. In other fusion systems the PQNT effect does not appear. As a result, this phenomenon is not assured whether it is related to the PQNT effect or other reaction mechanisms. Theoretically, many models have been used to reproduce the fusion process such as the quantum molecular dynamic model [18], the time-dependent Hartree-Fock method [19], the simplified semiclassical model [20], and the quantum diffusion approach [21], etc. In these studies, energy balance of the fusion Q value is generally neglected, which is equivalent to a tacit assumption of fusion Q value with zero. However, the effect of fusion Q value seems to be indispensable for sub-barrier fusion consideration. Fusion excitation functions for two hypothetical fusion systems with similar barrier heights but different fusion Q values are schematically shown in Fig. 1. It is obvious that the excitation functions converge to zero when the energy threshold is equal to $-Q$. It can be seen in Fig. 1 that at low enough energy, the fusion excitation function, due to its general properties, will be always larger for the system having the lower threshold. Here we neglect rare instances of resonancelike shape of the fusion excitation function. In a recent work, the new systematics take into account the Q value of heavy-ion fusion as an indispensable factor to understand the fusion process [22]. The reduced energy has been introduced, $E_r = \frac{E_{\mathrm{c.m.}}+Q}{V_c+Q}$, where $E_{\mathrm{c.m.}}$ is the incident energy of fusion system in the center of mass frame and V_c is the barrier height. An inclusion of this structural parameter allows one to remove an apparent paradox of nonenergy conservation for the fusion at energies deeply under the barrier. Many of the fusion data could be reduced to a quasiuniversal energy function by means of a simple energy scaling with the fusion Q value included explicitly. The new fusion excitation functions of the selected fusion systems follow a similar band and there is a systematic trend that can describe the sub-barrier fusion process. Within this approach, the sub-barrier fusion cross section can be easily predicted. The only variable parameter in the new energy scaling is the Coulomb barrier height. The requirement of universal or at least very similar shape of fusion excitation curves for many fusion systems determines specific values of the barrier heights. Here we could treat these values as experimental ones for sub-barrier fusion. The Coulomb potential can be accurately calculated, the nuclear interaction can be provided on the ground of nuclear models. Therefore, the Coulomb barrier height V_c can be entered into this new energy scaling formula [22]; the reduced fusion excitation functions can be obtained through various models and systematically compared with the experimental fusion excitation functions. According to these compared results, we can know which model gives a Coulomb barrier height which is suitable for the sub-barrier fusion systematics.

*zgl@buaa.edu.cn

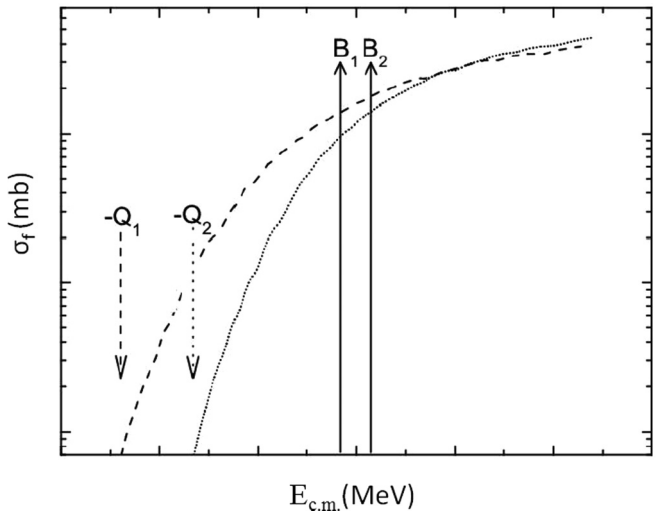

FIG. 1. General shape of the fusion excitation functions for two hypothetical fusion systems with similar barrier heights $B1$ and $B2$, and different fusion energy thresholds $-Q1$ and $-Q2$. Q stands for fusion Q values.

In this paper several generally used models including the Bass model, three modified proximity potential models, and the double folding model are introduced to calculate the nuclear potential. Then the Coulomb barrier heights which are obtained from these five models can be used in the new energy scaling formula to give the reduced fusion excitation functions which are compared with the reduced experimental data of many fusion systems. We also systematically explore which model is suitable for the calculation of the Coulomb barrier height among them.

This paper is organized as follows. In Sec. II the calculation process is introduced including several models. In Sec. III the calculation results and discussion are displayed. The conclusion is given in Sec. IV.

II. CALCULATION PROCESS

It is known that in the fusion process a new energy scaling was given by [22]

$$E_r = \frac{E_{\text{c.m.}} + Q}{V_c + Q}, \tag{1}$$

where $E_{\text{c.m.}}$ is the incident energy of fusion system in center of mass frame and the Coulomb barrier is defined as $V_c = \frac{Z_p Z_t e^2}{R}$, where Z_p and Z_t represent the charge numbers of projectile and target nuclei, respectively, $e^2 = 1.44$ MeV fm, $R = r_0(A_p^{1/3} + A_t^{1/3})$, where A_p and A_t stand for the mass numbers of projectile and target nuclei, respectively; r_0 is the reduced radius. So we can use these formulas to reduce the experimental fusion excitation functions. The barrier heights V_c which are treated as sub-barrier experimental ones are obtained using the scaling formula given above. The formula is not a unique one. If one would use another definition of energy reduced parameter E_r also with the fusion Q value, the resulting barrier heights could be different with respect to those discussed here.

Theoretically, in the fusion process the total interaction potential $V(R)$ between projectile and target nuclei is given by

$$V(R) = V_N(R) + V_C(R) + \frac{l(l+1)\hbar^2}{2\mu R^2}, \tag{2}$$

where the last term is the centrifugal potential. $\mu = \frac{m_p m_t}{m_p + m_t}$ represents the reduced mass of the fusion system, m_p and m_t denote the masses of projectile and target nuclei in the unit of MeV/c^2, respectively. l represents the angular momentum of the fusion system. Here we calculate the fusion cross section by adding centrifugal terms to the $l = 0$ barrier parameters. $V_N(R)$ stands for the nuclear potential and $V_C(R)$ is the Coulomb potential which is calculated by

$$V_C(R) = Z_1 Z_2 e^2 \begin{cases} \frac{1}{R} & (R > R_c), \\ \frac{1}{2R_c}\left[3 - \left(\frac{R}{R_c}\right)^2\right] & (R < R_c). \end{cases} \tag{3}$$

Here $R_c = 1.24(R_1 + R_2)$, $R_i = 1.28A_i^{1/3} - 0.76 + 0.8A_i^{-1/3}$ $(i = 1,2)$ corresponds to the radii of projectile and target nuclei. Then the Coulomb barrier height V_c can be extracted by using the conditions

$$\left.\frac{dV(R)}{dR}\right|_{R=R_B} = 0 \quad \text{and} \quad \left.\frac{d^2V(R)}{dR^2}\right|_{R=R_B} \leqslant 0. \tag{4}$$

The extracted V_c is entered into Eq. (1) to reduce the experimental fusion excitation functions. The reduced fusion excitation functions can be obtained. The systematic trend of reduced fusion excitation functions can be compared with that directly obtained from Eq. (1). These models can be tested from the experimental data.

For the $V_N(R)$ calculation, the Bass model [8] was selected first, which is a classical potential model for heavy-ion fusion reaction. The nuclear part of this model is derived from the liquid drop model, including the effects of the finite range of nuclear forces. The nuclear potential is defined with the difference in surface energies between finite and infinite separation s [23],

$$V_N(s) = -4\pi\gamma \frac{R_1 R_2}{R_{12}} f(s), \tag{5}$$

where R_1 and R_2 are radii of projectile and target nuclei, respectively. R_{12} is the reduced radius of the reaction system. $f(s)$ is the universal function of the separation coordinate s which does not depend on properties of the fragments involved. $f(s) = d \times \exp(-\frac{s}{d})$. Defining $R_i = r_0 A_i^{1/3}$ $(i = 1,2$ for projectile and target nuclei, respectively) and $4\pi R_i^2 \gamma = a_s A_i^{2/3}$. Then

$$V_N(r) = -\frac{d a_s A_1^{1/3} A_2^{1/3}}{R_{12}} \exp\left(-\frac{s}{d}\right), \tag{6}$$

where $d = 1.35$ fm which is based on interaction and fusion barriers, $r_0 = 1.07$ fm which is based on electron scattering data, and $a_s = 17$ MeV which is based on ground-state masses.

According to the original version of proximity [9], The nuclear potential between two surfaces of two nuclei is given

by

$$V_N^{\rm Prox}(R) = 4\pi\gamma b\bar{R}\phi\left(\frac{R-C_1-C_2}{b}\right). \quad (7)$$

Here the surface energy coefficient γ which is from Lysekil mass formula is given by

$$\gamma = \gamma_0[1-k_s I^2] \quad (8)$$

with $I = \frac{N-Z}{A}$. $N = N_1 + N_2$, $Z = Z_1 + Z_2$, and $A = A_1 + A_2$; N_i, Z_i and A_i $(i = 1,2)$ refer to the neutron, proton, and mass numbers of projectile and target nuclei, respectively. Both the surface energy constant γ_0 and the surface asymmetry constant k_s were first parametrized by Myers and Światecki by fitting the experimental binding energies [24]. After that, the values were revised. Therefore, most of the modified proximity potentials used the different parameter γ.

Second, the proximity potential Prox77 is selected with $\gamma_0 = 0.9517$ MeV/fm^2 and $k_s = 1.7826$ [25] to calculate $V_N(R)$. The mean curvature radius $\bar{R}$ is calculated by

$$\bar{R} = \frac{C_1 C_2}{C_1 + C_2}. \quad (9)$$

Here

$$C_i = R_i\left[1-\left(\frac{b}{R_i}\right)^2\right] \quad (i = 1,2), \quad (10)$$

where the radius $R_i = 1.28A_i^{1/3} - 0.76 + 0.8A_i^{-1/3}$ $(i = 1,2)$. The universal function $\phi(\xi)$ is written as

$$\phi(\xi) = \begin{cases} -\frac{1}{2}(\xi-2.54)^2 - 0.0852(\xi-2.54)^3 & (\xi \leqslant 1.2511), \\ -3.437\exp\left(-\frac{\xi}{0.75}\right) & (\xi \geqslant 1.2511). \end{cases} \quad (11)$$

Here $\xi = (r - C_1 - C_2)/b$ and the width parameter b is close to unity.

Third, the proximity potential Prox88 is selected [10] which was modified by using the more precise mass formula of Möller and Nix. The formulas are the same as that of the above Prox77 besides the surface energy constant $\gamma_0 = 1.2496$ and the surface asymmetry constant $k_s = 2.3$. This set of coefficients gives the stronger attraction in comparison with the above set of Prox77.

Recently, Myers and Światecki considered to remove the discrepancy between Prox77 and the experimental data (empirical barrier heights) which were obtained to compare with the measured fusion excitation function to calculated curves. They modified Eq. (7) by using their droplet model concept to obtain a new proximity potential named Prox00. Fourth, the proximity potential Prox00 is selected [11]. According to the droplet model, the matter radius C_i has the form

$$C_i = c_i + \frac{N_i}{A_i}t_i \ (i = 1,2). \quad (12)$$

Here the half-density radius c_i of the charge distribution has the form

$$c_i = R_{00i}\left(1 - \frac{7b^2}{R_{00i}^2} - \frac{49b^4}{8R_{00i}^4}\right)(i = 1,2), \quad (13)$$

with the nuclear charge radius

$$R_{00i} = 1.256A_i^{1/3}\left[1 - 0.202\left(\frac{A_i - 2Z_i}{A_i}\right)\right], \quad (14)$$

and neutron skin of nucleus

$$t_i = \frac{3}{2}r_0\left[\frac{JI_i - \frac{1}{12}gZ_iA_i^{-1/3}}{Q + \frac{9}{4}A_i^{-1/3}}\right](i = 1,2), \quad (15)$$

where r_0 is 1.14 fm, the nuclear symmetric energy coefficient $J = 32.65$ MeV, and $g = 0.757\,895$ MeV, the neutron skin stiffness coefficient $Q = 35.4$ MeV. The surface energy coefficient γ is given by

$$\gamma = \frac{1}{4\pi r_0^2}\left[18.63 - Q\frac{\left(t_1^2 + t_2^2\right)}{2r_0^2}\right]. \quad (16)$$

The universal function $\phi(\xi)$ is written as

$$\phi(\xi) = \begin{cases} -0.1353 + \sum_{n=0}^{5}[c_n/(n+1)](2.5-\xi)^{n+1} & (0 < \xi \leqslant 2.5), \\ -0.0955\exp\left(\frac{2.75-\xi}{0.7176}\right) & (\xi \geqslant 2.5). \end{cases} \quad (17)$$

The different values of constant c_n are $c_0 = -0.1886$, $c_1 = 0.2628$, $c_2 = -0.152\,16$, $c_3 = -0.045\,62$, $c_4 = 0.069\,136$, and $c_5 = -0.011\,454$.

Finally, the double folding model (DFM) is used to calculate the nuclear potential. The detailed process of DFM was shown in Refs. [15,26]. In the double folding model the nuclear potential V_N is given by

$$V_N(R) = \iint \rho_1(\mathbf{r_1})v(\mathbf{s} = |\mathbf{R} + \mathbf{r}_2 - \mathbf{r}_1|)\rho_2(\mathbf{r_2})\mathbf{dr_1}\mathbf{dr_2}, \quad (18)$$

where $\rho_1(r_1)$ and $\rho_2(r_2)$ denote the matter density distribution functions of projectile and target nuclei, respectively, which can be described by the spherically symmetric Fermi function,

$$\rho_{1(2)}(r) = \rho_0/[1 + \exp((r - c)/a)], \tag{19}$$

where the half-density radius c is followed as [27,28]

$$c = r_\rho\left(1 - \pi^2 a^2/3r_\rho^2\right), \tag{20}$$

with $r_\rho = 1.13A_i^{1/3}$ and the density diffuseness $a \approx 0.54$ fm, and A_i is the mass number of ith nucleus. The value of ρ_0 is determined by normalization so that

$$\int \rho_{1(2)}(\mathbf{r})d\mathbf{r} = A_i. \tag{21}$$

The NN interaction $v(s)$ between two nucleons in Eq. (18) is given by density-dependent $CDM3Y6$ interaction which can reproduce the basic properties of nuclear matter.

III. RESULTS AND DISCUSSION

The values of the Coulomb barrier heights provided by the considered models are presented in Table I. In the last column of Table I the values of the Coulomb barrier heights are obtained from optimized experimental data by Eq. (1). It is obviously observed in Table I that for light projectiles the difference among each model is smaller than that for heavier ones. What is more, the values of our barrier heights are systematically higher than those provided by any other models. The DFM gives the smallest Coulomb barrier heights and the values given by Bass model are between our barrier heights and the barrier height deduced from proximity potentials. The three types of proximity potentials show different behaviors. For ^{32,36}S + A and ^{40,48}Ca + A systems the results of Prox00 and Prox77 are almost similar, However, those of Prox88 are a little smaller in comparison with them, except ^{40,48}Ca + ^{124,132}Sn systems in which the results of Prox00 and Prox88 are similar and those of Prox77 are a little larger. However, for O + A systems the difference between Prox77 and Prox88 is smaller than that between Prox00 and Prox77. For Ni + A systems the difference between Prox00 and Prox88 is small; the values of Prox77 are a little higher in comparison with that of Prox00 and Prox88. All in all, there is a small difference among three types of proximity potentials. The values deduced from Prox00 are closest to our energy scaling values. In the present survey ^{18}O + Ni data are included. One should keep in mind that these data demonstrate the opposite trend to the Q-value rule for the fusion cross sections below the barrier. The fusion cross sections are lower for systems of higher Q values. The data seem to follow rather Q values of $2n$ transfer with the highest cross section for the highest $2n$ Q value. It is an open question whether this behavior is due to a limitation of fusion Q-value rule for light systems or due to the quality of the data. It would be interesting to extend the cross section data from the present level of 10 mb down to 1 mb or below, if possible. An application of the energy scaling procedure for these systems causes the corresponding barrier heights to be rather different; see Table I. Other fusion systems with equal Z_1 and Z_2 demonstrate almost the same sub-barrier fusion barrier heights; see Table I, for example Ca+Zr and Ni+Ni systems. The barrier heights obtained via our method for ^{32,36}S and ^{40,48}Ca on the same target are almost equal, which differ from all other predictions by other models. A region of the heavy nuclei fusions with ^{40}Ca ions gives larger Q values than that with ^{48}Ca ions. It is known that the ^{48}Ca nucleus is especially convenient for the production of super-heavy residues. These experiments are done with energies a little above the barrier yielding a compound nucleus at relatively low excitation energies. Maybe high Q-fusion values facilitate preserving the compound nuclei process, not fission compound nuclei. According to our systematics the sub-barrier fusion

TABLE I. The values of the obtained Coulomb barrier heights through Bass model (second column), double folding model (DFM) (sixth column), and three different types of proximity potential models (Prox00, Prox77, and Prox88 correspond to the third, fourth, and fifth columns, respectively). The first column denotes the different reaction systems. The values obtained by the new energy scaling are shown in the last column.

Reactions	Bass (MeV)	Prox00 (MeV)	Prox77 (MeV)	Prox88 (MeV)	DFM	V_C
^{32}S + ^{90}Zr	81.13	84.53	84.11	82.59	77.91	87.99
^{32}S + ^{96}Zr	80.09	83.27	83.04	81.58	76.99	88.75
^{32}S + ^{110}Pd	90.58	93.59	93.55	91.99	87.25	99.34
^{36}S + ^{90}Zr	79.61	82.58	82.57	81.11	76.63	89.38
^{36}S + ^{96}Zr	78.61	81.39	81.55	80.16	75.75	88.27
^{36}S + ^{110}Pd	88.93	91.53	91.91	90.42	85.86	98.85
^{40}Ca + ^{90}Zr	99.54	102.55	102.82	101.05	95.94	107.71
^{40}Ca + ^{96}Zr	98.28	101.07	101.53	99.84	94.83	107.54
^{40}Ca + ^{124}Sn	118.73	120.83	121.88	120.03	114.89	127.22
^{40}Ca + ^{132}Sn	117.22	119.12	120.40	118.66	113.55	129.11
^{48}Ca + ^{90}Zr	96.58	98.96	99.84	98.21	93.41	107.73
^{48}Ca + ^{96}Zr	95.40	97.58	98.64	97.10	92.36	106.45
^{48}Ca + ^{124}Sn	115.35	116.85	118.57	116.87	112.00	124.73
^{48}Ca + ^{132}Sn	113.93	115.26	117.19	115.56	110.73	123.89
^{16}O + ^{154}Sm	61.10	64.71	62.93	61.89	58.33	66.26
^{16}O + ^{148}Sm	61.64	65.38	63.46	62.37	58.80	66.86
^{16}O + ^{144}Sm	62.01	65.84	63.83	62.71	59.13	67.27
^{16}O + ^{186}W	70.83	74.30	72.55	71.45	67.82	79.94
^{16}O + ^{58}Ni	31.80	35.54	33.32	32.51	29.82	36.90
^{16}O + ^{60}Ni	31.58	35.23	33.08	32.29	29.65	38.25
^{16}O + ^{62}Ni	30.46	34.93	32.87	32.08	29.47	37.18
^{16}O + ^{64}Ni	31.18	34.65	32.66	31.89	29.31	38.17
^{18}O + ^{58}Ni	31.21	34.54	32.70	31.93	29.38	37.10
^{18}O + ^{60}Ni	31.00	34.25	32.48	31.72	29.20	38.95
^{18}O + ^{64}Ni	30.61	33.70	32.08	31.35	28.88	39.80
^{16}O + ^{76}Ge	34.80	38.29	36.38	35.58	32.82	43.06
^{18}O + ^{74}Ge	34.36	37.53	35.95	35.16	32.50	42.66
^{18}O + ^{118}Sn	50.50	53.84	52.36	51.39	48.14	57.77
^{58}Ni + ^{58}Ni	99.24	102.42	102.75	100.91	95.57	107.73
^{58}Ni + ^{64}Ni	97.48	100.30	100.91	99.16	94.05	107.11
^{64}Ni + ^{64}Ni	95.78	98.28	99.18	97.52	92.58	107.69
^{58}Ni + ^{132}Sn	158.63	158.82	161.75	159.59	154.11	169.79
^{64}Ni + ^{118}Sn	159.54	159.76	162.63	160.37	154.98	167.25
^{64}Ni + ^{132}Sn	156.08	156.00	159.30	157.24	151.90	164.69
^{64}Ni + ^{124}Sn	158.00	158.08	161.14	158.95	153.61	167.51
^{58}Ni + ^{124}Sn	160.63	160.99	163.68	161.39	155.88	169.95

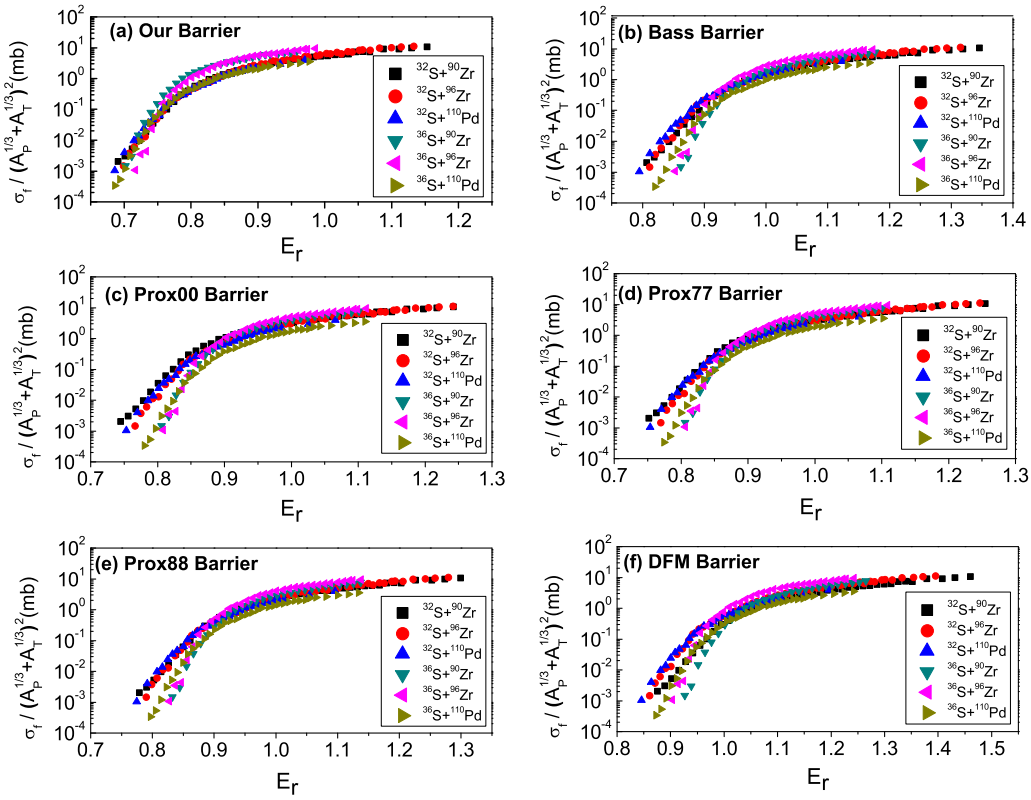

FIG. 2. (Color online) The reduced fusion excitation functions in terms of the reduced energy parameter E_r for $^{32,36}S + {}^{90,96}Zr, {}^{32,36}S + {}^{110}Pd$ systems. (a) From our new energy scaling; (b) from Bass model; (c) from Prox00; (d) from Prox77; (e) from Prox88; (f) from DFM.

should be larger for ^{40}Ca than that in the ^{48}Ca case. Existing experimental data such as Ca + Pb fusion systems seem to demonstrate the opposite trend.

Figures 2–4 show the reduced experimental fusion excitation functions from our new energy scaling with the barrier heights obtained from the above models. The fusion cross sections are reduced through $\sigma_f/(A_p^{1/3} + A_t^{1/3})^2$ to eliminate the geometric effect of fusion systems and the energy is reduced by the new energy scaling of Eq. (1). The horizontal axis represents the reduced energy parameter E_r through Eq. (1). Figure 2 shows the results of $^{32,36}S + {}^{90,96}Zr, {}^{110}Pd$ systems. It can be seen that our new energy scaling gives a similar shape for all excitation functions. In comparison with our distribution which is shown in Fig. 2(a), it is observed that the reduced fusion excitation functions given by our new energy scaling almost keeps the same shape. The data obtained through other models are more scattered than those obtained by our new energy scaling. The results of the Bass model and the DFM show the larger deviation at the region of the sub-barrier energies. However, those of three types of proximity potentials (Prox00, Prox88, and Prox77) show the small deviation, especially for Prox77. As a result, the proximity potential model can give the reasonable barrier height.

The reduced experimental fusion excitation functions of the $^{40,48}Ca + A$ systems are shown in Fig. 3. The phenomenon is similar as in Fig. 2. Our new energy scaling also shows a similar shape for all of fusion excitation functions. At the sub-barrier energy region, in comparison with Fig. 3(a), the results of Figs. 3(b) and 3(f) show a larger deviation than those of the other models. Those of the three types of proximity potentials have a smaller deviation except that of Prox00 for the $^{48}Ca + {}^{132}Sn$ system has a little larger deviation. It is indicated that the proximity potential model can reasonably calculate the barrier height for most of the fusion systems. In Figs. 2 and 3 several fusion systems with the same target nuclei are selected. However, the masses of projectiles $^{40,48}Ca$ are larger than that of $^{32,36}S$. With respect to Fig. 2, at the sub-barrier energy region the band of fusion excitation functions for $^{40,48}Ca$ are thinner. It seems that with the increase of projectile mass, the trends of all excitation functions are easily close to similarity.

In Fig. 4 the reduced experimental fusion excitation functions of O + A systems are shown. In comparison with Fig. 4(a), we can see that the results of the Bass model show a larger deviation. Those of the three types of proximity potential models and the DFM show a smaller deviation. If the influence of $^{16}O + {}^{76}Ge$ and $^{18}O + {}^{74}Ge$ is not considered, Prox00 can provide a good shape with respect to the shape of our new energy scaling. In comparison with Figs. 2 and 3, at the sub-barrier energy region the bandwidth is larger and the projectile ^{16}O is lighter than $^{32,36}S$ and $^{48,48}Ca$. It also seems that with the decrease of projectile mass, the band easily inclines to be scattered.

From Figs. 2–4 we can see that our new energy scaling can give a similar shape. It is indicated that when considering the Q value, fusion shows a characteristic of compound

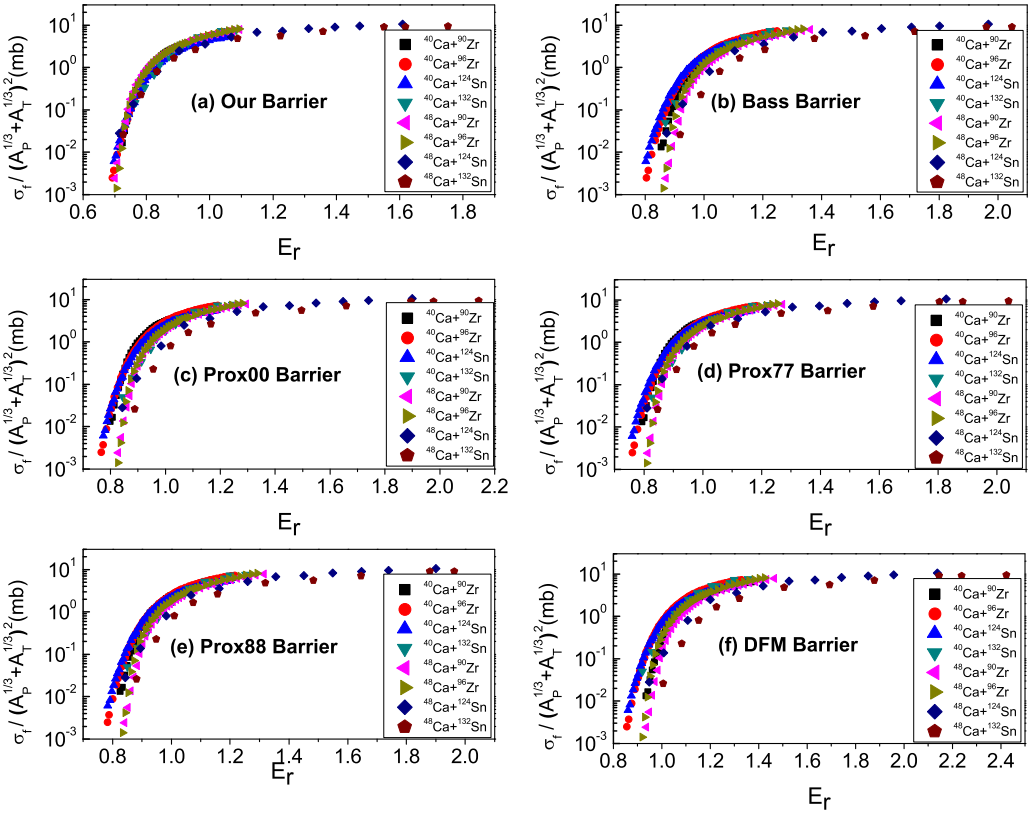

FIG. 3. (Color online) Same as Fig. 2 for ^{40,48}Ca + ^{90,96}Zr, ^{40,48}Ca + ^{124,132}Sn systems.

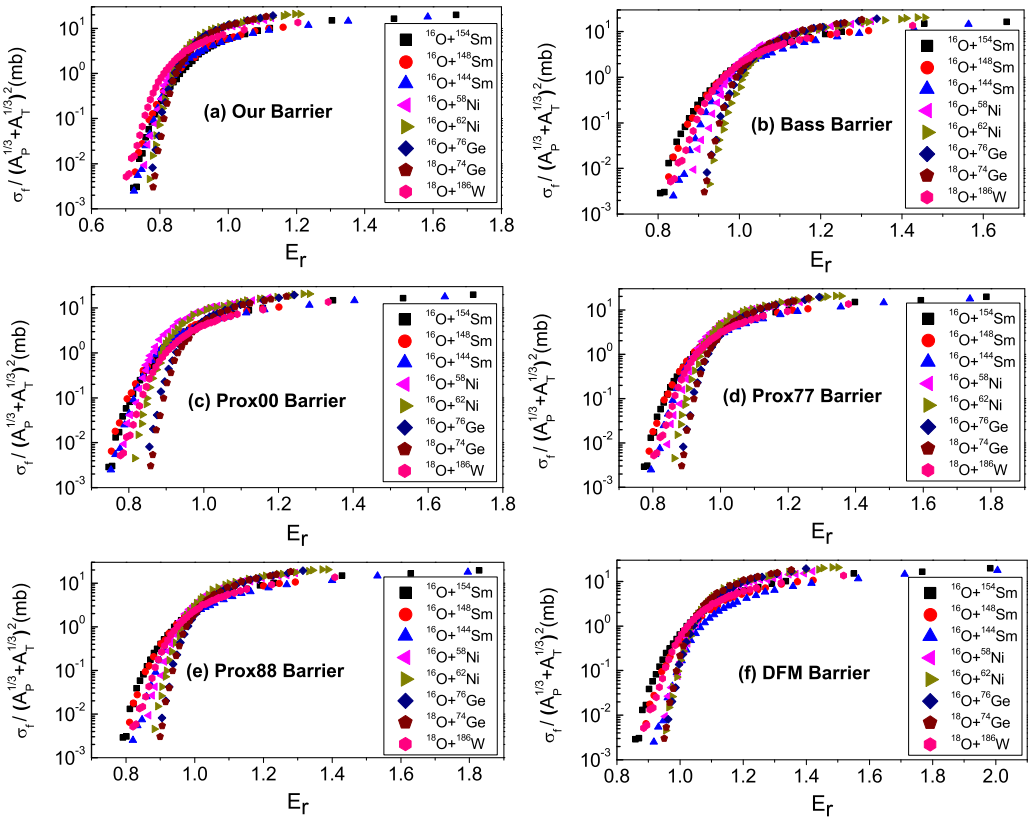

FIG. 4. (Color online) Same as Fig. 2 for ^{16}O + ^{58,62}Ni, ^{16,18}O + ^{76,74}Ge, ^{16,17}O + ^{144,148,154}Sm, ^{16}O + ^{186}W systems.

nucleus. We can state that our "experimental" barrier height is an effective parameter for enhancement reduction, whereas the barrier heights obtained from the various models only describe entrance channel properties. Moreover, it is observed in our treatment of the reduced experimental fusion excitation function that the barrier heights of systems with the $Z_P \times Z_T$ product are the same independent on masses of interacting isotope nuclei. This feature of the sub-barrier fusion is not reproduced by the discussed models. However, in comparison with the results of our new energy scaling, the proximity potential model can almost reproduce this trend except in heavy fusion systems. Moreover, with the increase of projectile mass, the deviation of the band decreases. However, the Bass model and the DFM show a large deviation. It is well known that the universal function of the Bass model is straight along with s. It shows a large deviation respective to the empirical data, moreover, it falls off too slowly at large distances s. However, that of proximity potential models shows a curve which reproduces the empirical data quite well on the average. As a result, the fusion excitation functions of the Bass model show a large deviation with respect to the experimental data. On the contrary, the results of proximity potential models are closer than that of Bass model. For the double folding potential, it is obtained by folding the nucleon density distribution of the projectile and target nuclei with a standard density-dependent Yukawa-type nucleon-nucleon interaction. The calculation neglects the saturating properties of nuclear forces and produces the potential which is too deep, especially at the small separations s relevant to the fusion problem. Thus the calculated barrier heights are lowered.

IV. CONCLUSION

The Bass model, three types of proximity models (Prox00, Prox88, and Prox77), and the DFM are introduced to calculate the nuclear potential. Then the Coulomb barrier heights can be obtained through different models for different fusion systems. According to our new energy scaling, by using the Coulomb barrier heights given by these models, the reduced experimental fusion excitation functions can be systematically obtained to compare with that by our new energy scaling. According to the comparison, it is shown that our new scaling method produces the highest barrier heights and the double folding model gives the lowest barrier heights. The proximity potential model can give reasonable Coulomb barrier heights in comparison with the experimental fusion excitation functions. This method tests the availability of the model for calculating the fusion barrier heights. It can be used as a guideline for estimating the fusion barrier height of those cases in which the measurements do not exist or the studies need to be further explored.

ACKNOWLEDGMENTS

This work was supported by the National Nature Science Foundation of China under Grants No. 11475013, No. 11035007, No. 11175011, and State Key Laboratory of Software Development Environment (SKLSDE-2014ZX-08), as well as by the Key Laboratory of High Precision Nuclear Spectroscopy, Institute of Modern Physics, Chinese Academy of Sciences. W.W.Q. is grateful to the Innovation Foundation of BUAA for Ph.D. Graduates.

[1] J. R. Leigh *et al.*, Phys. Rev. C **52**, 3151 (1995).
[2] Z. H. Liu and J. D. Bao, Chin. Phys. Lett. **21**, 1491 (2004).
[3] Z. H. Liu and H. Y. Zhou, Chin. Phys. **16**, 2338 (2007).
[4] B. B. Back, H. Esbensen, C. L. Jiang, and K. E. Rehm, Rev. Mod. Phys. **86**, 317 (2014).
[5] C. Signorini, Nucl. Phys. A **735**, 329 (2004).
[6] J. J. Kolata *et al.*, Phys. Rev. C **57**, R6(R) (1998).
[7] R. Graeger *et al.*, Phys. Rev. C **81**, 061601(R) (2010).
[8] R. Bass, Nucl. Phys. A **231**, 45 (1974).
[9] J. Blocki, J. Randrup, W. J. Światecki, and C. F. Tsang, Ann. Phys. (NY) **105**, 427 (1977).
[10] W. Reisdorf, J. Phys. G: Nucl. Part. Phys. **20**, 1297 (1994).
[11] W. D. Myers and W. J. Światecki, Phys. Rev. C **62**, 044610 (2000).
[12] G. L. Zhang and X. Y. Le, Chin. Phys. C **32**, 312 (2008).
[13] I. Dutt and R. K. Puri, Phys. Rev. C **81**, 064608 (2010).
[14] I. Dutt and R. K. Puri, Phys. Rev. C **81**, 064609 (2010).
[15] W. W. Qu, G. L. Zhang, and X. Y. Le, Nucl. Phys. A **868-869**, 1 (2011).
[16] P. Jacobs, Z. Fraenkel, G. Mamane, and I. Tserruya, Phys. Lett. B **175**, 271 (1986).
[17] A. M. Stefanini *et al.*, Phys. Rev. C **73**, 034606 (2006).
[18] N. Wang, Z. Li, X. Wu, J. Tian, Y. X. Zhang, and M. Liu, Phys. Rev. C **69**, 034608 (2004).
[19] R. Keser, A. S. Umar, and V. E. Oberacker, Phys. Rev. C **85**, 044606 (2012).
[20] V. I. Zagrebaev, Phys. Rev. C **67**, 061601(R) (2003).
[21] V. V. Sargsyan, G. G. Adamian, N. V. Antonenko, W. Scheid, and H. Q. Zhang, Eur. Phys. J. A **49**, 54 (2013).
[22] R. Wolski, Phys. Rev. C **88**, 041603(R) (2013).
[23] R. Bass, *Nuclear Reactions with Heavy Ions* (Springer-Verlag, Berlin, 1980), pp. 324–340.
[24] W. D. Myers and W. J. Światecki, Nucl. Phys. **81**, 1 (1966).
[25] W. D. Myers and W. J. Światecki, Ark. Fys. **36**, 343 (1967).
[26] D. N. Basu, Phys. Lett. B **566**, 90 (2003).
[27] D. K. Srivastava, N. K. Ganguly, and P. E. Hodgson, Phys. Lett. B **51**, 439 (1974).
[28] D. K. Srivastava, D. N. Basu, and N. K. Ganguly, Phys. Lett. B **124**, 6 (1983).